2012

Experimental Testing of an Organic Rankine Cycle with Scroll-Type Expander

Brandon J. Woodland
bwoodlan@purdue.edu

James E. Braun

Eckhard A. Groll

W. Travis Horton

Experimental Testing of an Organic Rankine Cycle with Scroll-type Expander

Brandon J. WOODLAND[1]*, James E. BRAUN[1], Eckhard A. GROLL[1], and W. Travis HORTON[1]

[1]Purdue University
School of Mechanical Engineering
Ray W. Herrick Laboratories
West Lafayette, Indiana, USA
Phone: 801-602-7382 Email: bwoodlan@purdue.edu

* Corresponding Author

ABSTRACT

An organic Rankine cycle (ORC) is a power cycle employing an organic working fluid. The term ORC is also applied generally to any Rankine cycle with a low-grade heat source (80° – 300°C). Because ORC are often employed in small-scale applications, use of positive displacement equipment is favored over the centrifugal units used in large-scale power plants. A key feature of a positive displacement expander is its built-in volume ratio.

An ORC with a scroll-type expander is studied experimentally. Data for steady state tests of the ORC are presented according to a proposed steady state standard. It is shown that the adiabatic efficiency of the expander can be fully characterized by its filling factor and the expansion volume ratio imposed across it. In particular, the peak adiabatic efficiency occurs near a filling factor of unity and an expansion volume ratio near the built-in volume ratio of the expander. The influence of the expander's performance on cycle efficiency is considered. A procedure is presented which allows prediction of cycle performance based on knowledge of the expander efficiency versus expansion volume ratio, cycle operating conditions, and working fluid. Using this procedure, an optimal expander can be chosen for a set of cycle operating conditions based on its peak efficiency and built-in volume ratio.

1. INTRODUCTION

An organic Rankine cycle (ORC) is a thermodynamic power cycle in which an organic working fluid is employed in place of the steam used in traditional Rankine cycles. The organic working fluid is typically used with a low-grade (80° – 300°C) heat source because it allows for higher condensing pressures and lower pressure ratios than steam. The term ORC is also applied generally to any Rankine cycle with a low-grade heat source. Another distinction between ORC and traditional Rankine cycles can be the size of the power plant. Whereas steam power plants are typically built on the MW scale, ORC applications often lie in the kW range. This small size prompts the selection of a positive displacement pump and expander in favor of the centrifugal units used in large-scale plants. A key feature of a positive displacement expander is that it expands at a fixed internal volume ratio. The internal volume ratio of the expander is an important design variable when a set of operating conditions for an ORC is considered.

Experimental results for an ORC using a positive displacement scroll-type expander with R134a as the working fluid are presented in this paper. The discussion of the results focuses on the expander built-in volume ratio and its suitability to the operating conditions of the ORC.

2. SYSTEM DESCRIPTION

A schematic of the test system is given in Figure 1. This figure shows the four main components of the ORC: the pump, evaporator, expander, and condenser. The pump moves the subcooled liquid working fluid through the cycle. It generates the high pressure needed to evaporate the working fluid close to the heat source temperature. The evaporator takes a heat source fluid on one side and transfers heat to the working fluid. The working fluid exits the

evaporator at a superheated vapor state where it enters the expander. The expander extracts work and drops the pressure and temperature of the working fluid as a result. The working fluid then condenses against the heat sink fluid at this low pressure where it leaves the condenser as a subcooled liquid and re-enters the pump. As seen in Figure 1, saturated steam was used as the heat source while municipal cold water was used as the heat sink for the cycle.

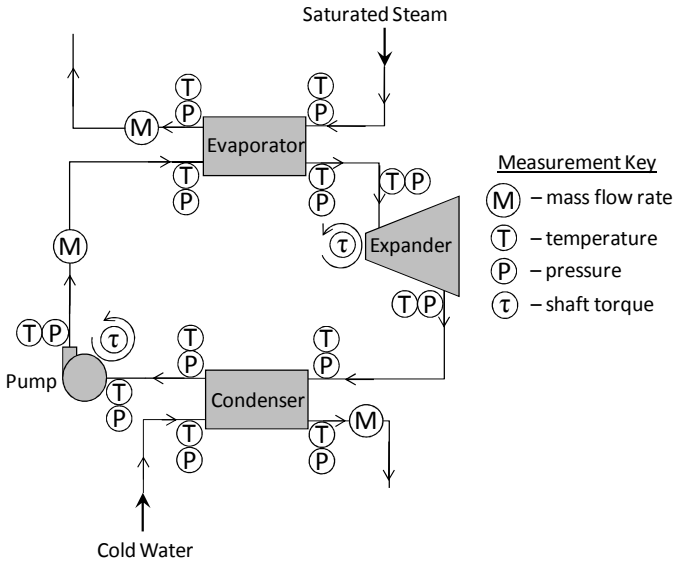

Figure 1: ORC system schematic showing the four major cycle components, heat source and sink fluids, and the measurements taken on the system

A description of each of the main components used in the test system follows in Table 1.

Table 1: Summary of main ORC component characteristics

Pump		
Three piston diaphragm	Maximum Discharge Pressure (kPa)	7000
	Capacity at Max Pressure (L/min)	11.3
	Delivery at Max Pressure (rev/L)	155
Condenser/Evaporator		
Brazed plate	Number of Plates	110
(single-pass, counterflow)	Volume per Side (L)	~6
Expander		
Automotive scroll compressor	Maximum Speed (RPM)	5000
(run in reverse as an expander)	Displacement (compressor mode) (cc)	104.8[a]
	Built-in Volume Ratio	~1.61[a]-1.8[b]
	Displacement (expander mode) (cc)	(~58.22[b]-65.09[a])[c]

[a] Bell, 2011; [b] Hugenroth, 2006; [c] Calculated from built-in volume ratio using Equation (2)

The expander was originally an automotive scroll compressor. To operate the machine as an expander, the high-pressure flow is introduced into the compressor discharge port. This required the removal of the discharge valve, which would have blocked the flow from entering the port. Another modification was to disable the radial compliance feature of the machine. With radial compliance, a minimum speed is required to generate sufficient centrifugal force for the scroll wraps to maintain contact. If it were not disabled, the leakage at lower speeds would be more severe. To disable the radial compliance, a dowel pin was pressed between the compliant mechanism and the crank shaft such that the scroll wraps just began to make contact.

There is a discrepancy in the built-in volume ratio of the expander according to two references in which research was performed using the same machine (Hugenroth, 2006; Bell, 2011). A value of 1.8 is assumed in this work.

3. TEST METHOD

3.1 Instrumentation and Layout

Figure 1 gives the type and location of each measurement on the system. Measurements were recorded one-at-a-time using a digital multi-meter and an armature relay multiplexer. The instrumentation used to obtain each measurement is given in Table 2.

Table 2: Instrumentation used to obtain system measurements

Measurement	Description	Accuracy
Temperature	Ungrounded T-type thermocouple	±0.22 K [a]
Pressure	Electronic pressure transducer (gauge)	±5.15 kPa [b]
Mass Flow (working fluid and steam)	Coriolis mass flow sensor	± 0.1% reading, reading > 0.151 kg/s [c] ± 1.51×10^{-4} kg/s, reading < 0.151 kg/s [c]
Mass Flow (cold water)	Coriolis mass flow sensor	± 0.5% reading, reading > 0.015 kg/s [c] ± 7.5×10^{-5} kg/s, reading < 0.015 kg/s [c]
Torque	Rotating torque sensor	± 0.07 N m (pump) [b] ± 0.17 N m (expander) [b]
Shaft Speed	Variable frequency motor controller analog output	± 3.42 RPM (pump) [d] ± 9.77 RPM (expander) [d]

[a] Maximum deviation from expected reading of all thermocouples with distilled ice water and distilled boiling water at measured atmospheric pressure (95% confidence assumed)
[b] Calibrated accuracy using RSS of calibration standard accuracy and linear curve fit 95% prediction interval (error in reading atmospheric pressure included for pressure transducers)
[c] Values reported by manufacturer (95% confidence assumed)
[d] ½ resolution based on 8 bit DAC and full scale value of 1750 RPM (pump) and 5000 RPM (expander) (95% confidence assumed)

A photograph of the test system is given in Figure 2 showing the physical layout of system components and instrumentation. The four main system components are placed on the same horizontal plane.

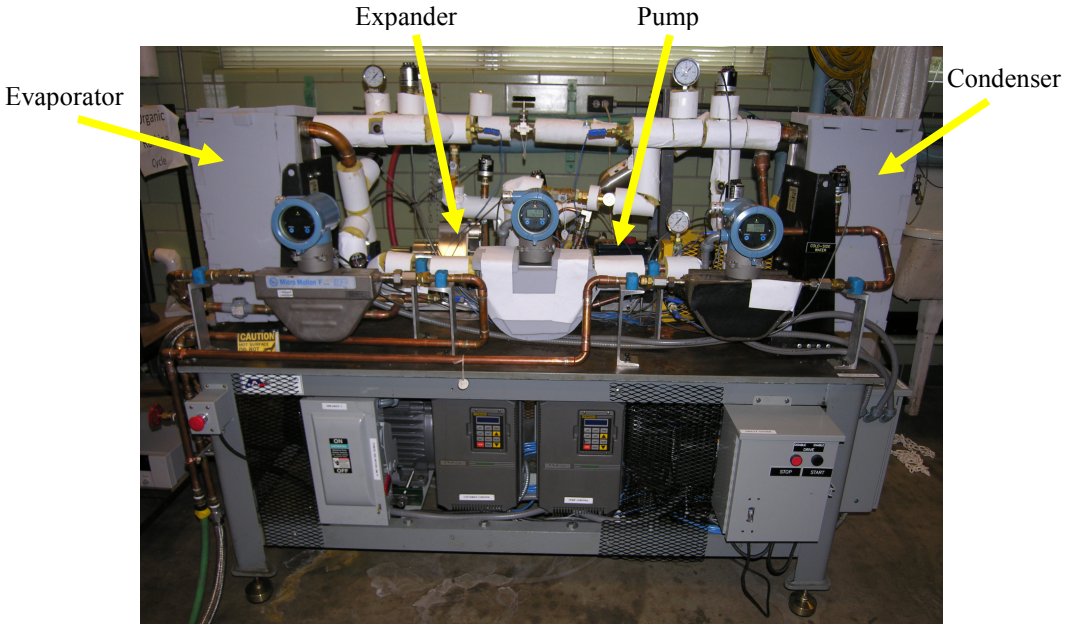

Figure 2: Photograph of ORC system

3.2 Steady State Standard

Several standards exist which define steady state conditions for vapor compression cycles used as air conditioners and heat pumps. However, to the authors' knowledge, there is no such standard for an ORC. For the purposes of this work, a standard is proposed which is summarized in Figure 3 and Table 3. A measurement is defined as one cycle of the multiplexer through the measurement channels of the system, resulting in one sample of each measurement shown in Figure 1. Measurements are recorded at a rate of approximately 1 Hz. As shown in Figure 3, an average is made of the 30 most recent measurements. This average is compared with an average of 30 measurements taken approximately 10 minutes (600 measurements) earlier. Then the difference or percent change between the two averages is computed and compared to the criteria given in Table 3.

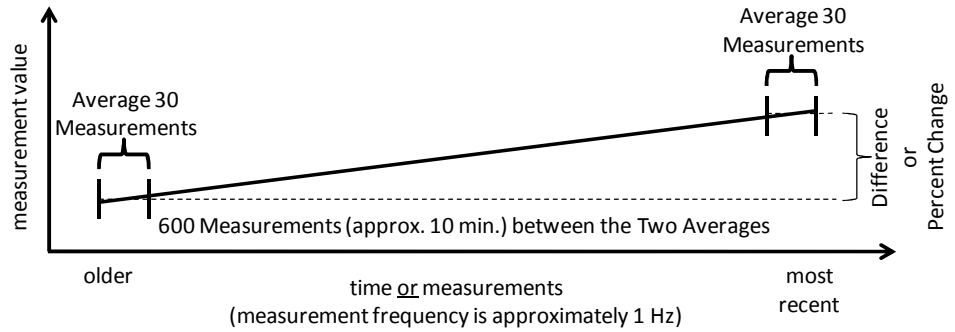

Figure 3: Diagram showing which measurements are averaged and the space between those averages used to determine steady state conditions

Table 3: Comparison criteria for each measurement for steady state conditions

Measurement	Steady State Criteria
Temperature	Difference < 0.5 K
Pressure	Change < 2%
Mass Flow	Change < 2%
Rotating Equipment Speed	Change < 2%

Steady state is reached when the criteria in Table 3 are satisfied for steam, working fluid, and cold water. Then the most recent 10 minutes of data (approximately 600 measurements) are averaged to produce steady state measurement values. These values are used to compute the results presented in this work.

Some exceptions were made to the steady state criteria under the following conditions which occurred occasionally:

1) Cold water pressure and flow rate did not satisfy the criteria due to uncontrollable pressure fluctuations in the municipal water line.
2) Measurements of the steam mass flow rate did not satisfy the criteria when it entered the mass flow meter as a saturated mixture because the mass flow meter cannot accurately measure two-phase flow.
3) The expander discharge temperature oscillated at extremely low flow rates of the working fluid, but no increasing or decreasing trend was observed in the oscillations.

3.3 System Inputs

All tests were run with saturated steam at the inlet to the evaporator with a temperature which varied between tests in the range of 117° – 97°C depending on the mass flow rate of organic working fluid running through the evaporator. The steam temperature generally remained constant throughout the evaporator because it did not fully condense. There are a few exceptions to this. Particularly when tests were run at high mass flow rates, the steam became slightly subcooled at the evaporator exit. The variation in steam mass flow rate could not be determined accurately because it predominantly entered the mass flow meter as a two-phase mixture. Cold water was run through the condenser at a constant mass flow rate, which varied between tests in the range of 0.587 – 0.673 kg/s with temperatures varying from 13° – 18°C. The fluctuations in these cycle inputs do not affect results that are specific to the expander. Their affect on cycle efficiency is sufficiently small for the arguments presented in this work.

4. RESULTS AND DISCUSSION

4.1 Definitions

Experimental results are presented with calculations according to the equations below. REFPROP (Lemmon *et al.*, 2012) was used where computation of fluid properties was required.

The expander filling factor (Lemort *et al.*, 2009) is defined analogously to volumetric efficiency for a compressor as

$$\phi_{ff} = \frac{\dot{m}_{wf} \cdot v_{suc}(T_{suc}, P_{suc})}{N_{shaft} \cdot V_{D,exp}} \tag{1}$$

where $V_{D,exp}$ is calculated for the expander as

$$V_{D,exp} = \frac{V_{D,comp}}{r_v} \tag{2}$$

according to Bell (2011).

For an expander, the filling factor is frequently greater than unity. This suggests leakage as a result of the pump delivering more flow than the expander takes into the expansion chamber with each revolution. Values below unity suggest that the expansion chamber is not being completely filled with each revolution.

The expansion volume ratio is defined as the ratio of working fluid specific volumes calculated from temperature and pressure measurements at the expander discharge and suction lines.

$$V_{ratio} = \frac{v_{dis}(T_{dis}, P_{dis})}{v_{suc}(T_{suc}, P_{suc})} \tag{3}$$

The expander adiabatic efficiency is defined as the measured shaft power out of the expander divided by the isentropic work of the working fluid between the expander suction and discharge pressures.

$$\eta_{exp} = \frac{\dot{W}_{exp,shaft}}{\dot{W}_s} \tag{4}$$

where

$$\dot{W}_{exp,shaft} = 2\pi \cdot \tau_{exp,shaft} \cdot N_{exp,shaft} \quad , \quad \dot{W}_s = \dot{m}_{wf}\left(h(T_{suc}, P_{suc}) - h(P_{dis}, s_{suc})\right) \tag{5}$$

The cycle thermal efficiency is defined as the measured net work out of the cycle over the measured heat input to the working fluid.

$$\eta_{cycle} = \frac{\dot{W}_{net,shaft}}{\dot{Q}_{in,wf}} \tag{6}$$

where

$$\dot{W}_{net,shaft} = \dot{W}_{exp,shaft} - \dot{W}_{pump,shaft} \quad , \quad \dot{Q}_{in,wf} = \dot{m}_{wf}\left(h(T_{evap,out}, P_{evap,out}) - h(T_{evap,in}, P_{evap,in})\right)\Big|_{wf} \tag{7}$$

and $\dot{W}_{pump,shaft}$ is computed analogously to $\dot{W}_{exp,shaft}$ according to Equation (5). It was not possible to use a heat input measurement from the steam side of the evaporator because the mass flow meter was unable to measure the steam as a saturated mixture as it exited the evaporator.

The Second Law efficiency of the cycle is given as

$$\eta_{cycle,II} = \frac{\eta_{cycle}}{\eta_{Carnot}} \tag{8}$$

where

$$\eta_{Carnot} = 1 - \frac{T_{cw,in} + 273.15}{T_{steam,in} + 273.15} \tag{9}$$

The uncertainty in the measured variables is computed with a 95% confidence interval using methods presented in Figliola and Beasley (2006) where the systematic uncertainty is given in Table 2. Uncertainty in fluid property routines is considered negligible relative to measurement uncertainties. Random uncertainty was quantified using

the measurements taken during the steady state interval. These uncertainties are propagated to a calculated result $R = f(x_1, x_2, ..., x_L)$ such that the uncertainty in the result is given as

$$u_R = \pm \left[\sum_{i=1}^{L} \left(\frac{\partial R}{\partial x_i} u_{x_i} \right)^2 \right]^{1/2} \tag{10}$$

where the partial derivatives are computed using a central difference scheme with a step size equal to the uncertainty in the measured variable. Implicit in Equation (10) is the assumption that systematic uncertainties are uncorrelated.

4.2 Experimental Results

The efficiency of an ORC is highly dependent on the performance characteristics of the expander. As with volumetric efficiency for compressors, the filling factor of an expander can give important insight into the expander's performance. Figure 4 gives the filling factor for the expander for all steady state tests performed.

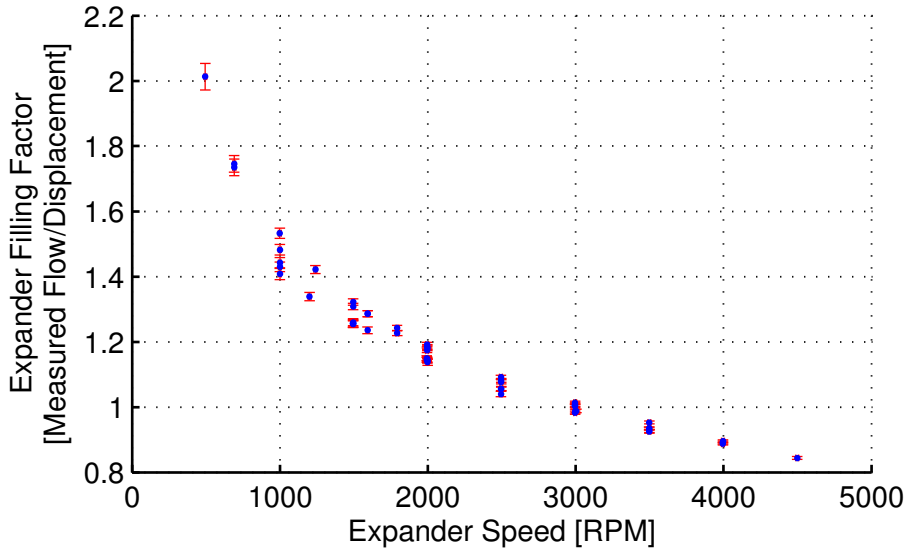

Figure 4: Filling factor versus shaft speed for the expander using R134a, built-in volume ratio of 1.8 assumed, error bars show 95% confidence interval

It can be seen from Figure 4 that, for the data collected, the filling factor is almost exclusively a function of the rotational speed of the expander. The slight spreading of the data is attributed to different expansion volume ratios imposed on the expander. A higher expansion volume ratio corresponds to a higher pressure difference and consequently, more leakage.

The influence of the filling factor and the expansion volume ratio on the adiabatic efficiency of the expander can be seen in Figures 5a and 5b. These figures show the promising adiabatic efficiencies that can be achieved using an off-the-shelf scroll machine that was not originally intended for use as an expander. As expected, the peak efficiency occurs when the filling factor is near unity. The efficiency drops off sharply for filling factors below unity, while the drop-off for filling factors above unity is less severe. This suggests that under-filling the expander is more detrimental to its performance than an equivalent amount of leakage. The spread in efficiencies for a given filling factor shown in Figure 5a is also due to different expansion volume ratios. The influence of expansion volume ratio on expander efficiency can be seen in Figure 5b, where the spread in the data is now due to differences in filling factor. As expected, the peak adiabatic efficiency occurs near the built-in volume ratio of the expander (Lemort *et al.*, 2009). The true maximum occurs at an expansion ratio slightly higher than the built-in volume ratio in order to compensate for suction pressure drop and leakage. As with Figure 5a for filling factor, Figure 5b shows a sharp drop in performance for expansion volume ratios below the built-in volume ratio. The drop-off is less severe for values above the built-in volume ratio. This suggests that over-expansion (resulting in recompression of the working fluid at the expander discharge port) is more detrimental than under-expansion. With this understanding of the impacts of filling factor and expansion volume ratio, the expander adiabatic efficiency can be fully characterized with a single contour plot given in Figure 6.

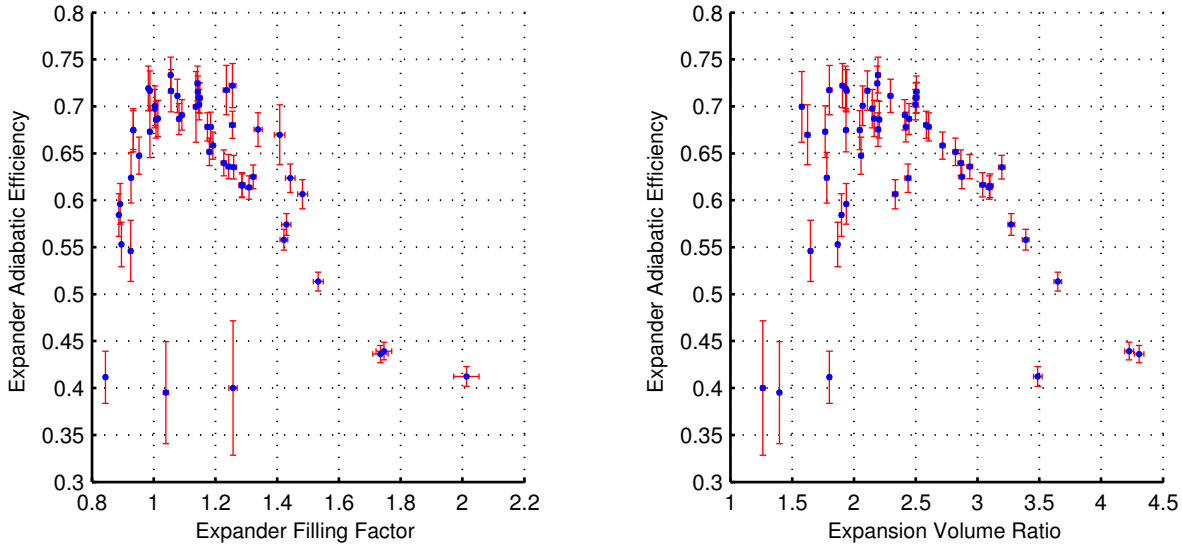

(a) (b)

Figure 5: Adiabatic efficiency versus filling factor (a) and volume expansion ratio (b) for the expander using R134a, built-in volume ratio of 1.8 assumed, error bars show 95% confidence interval

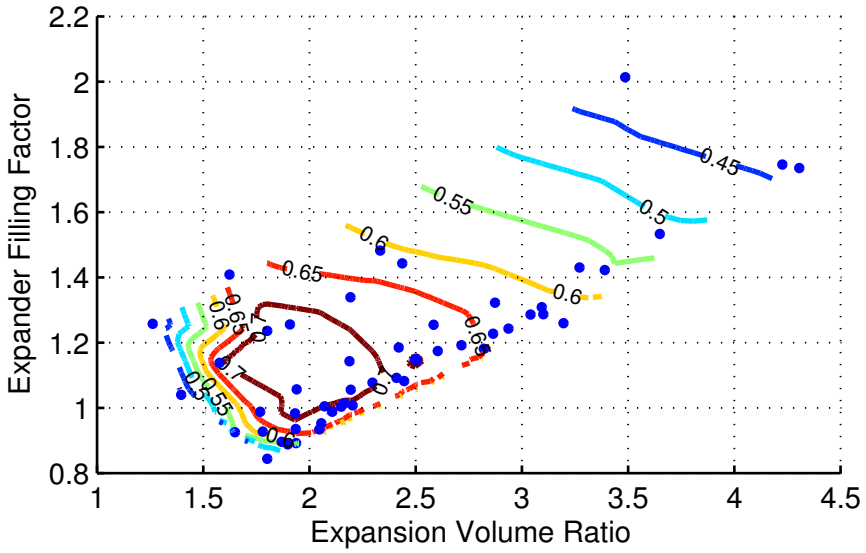

Figure 6: Expander adiabatic efficiency using R134a, contours show lines of constant adiabatic efficiency as a function of volume expansion ratio and filling factor

The data in Figure 6 is presented as lines of constant adiabatic efficiency plotted with respect to expansion volume ratio and expander filling factor. Dots indicate the steady state data points used to generate the contours. The contours correspond to a surface fit to the data using linear interpolation. At this point it can be seen that the slope of the drop-off at high expansion ratio in Figure 5b may be exaggerated. This is because the experimentally achievable data points at high volume ratio necessarily occurred at a high filling factor. The pump could not displace enough volume to achieve the same expander inlet densities at lower filling factors (where the expander speed was high). If data could be obtained for higher expansion volume ratios at filling factors closer to unity (using a larger pump), the drop-off in expander efficiency for higher expansion volume ratios would likely be less pronounced. A similar statement could be made for the drop-off at high filling factors in Figure 5a. In this case the minimum flow rate of the pump was not low enough to achieve low expansion ratios at high filling factors (where the expander speed was low). Despite these limitations in the data, a region of peak adiabatic efficiency in Figure 6 is still sufficiently developed.

It is instructive to study the interaction between the changing expander efficiency and the efficiency of the ORC. The Second Law efficiency for the ORC is given in Figure 7. The data is presented as lines of constant Second Law efficiency as a function of expansion volume ratio and expander adiabatic efficiency. Some noise can be observed in the contour lines of Figure 7 due to variations in the cycle inputs that could not be controlled (see Section 3.3).

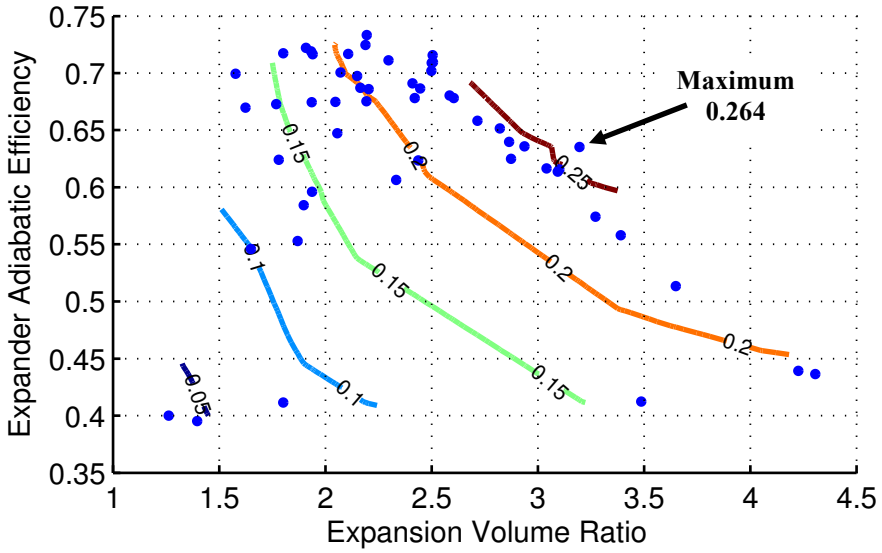

Figure 7: Cycle Second Law efficiency using the tested expander and R134a, contours show lines of constant Second Law efficiency as a function of expander volume ratio and expander adiabatic efficiency

The maximum Second Law efficiency achieved (0.264 ±0.004 [95%]) is denoted by the arrow. Finding the maximum cycle efficiency for a given expander and operating conditions is like solving an optimization problem subject to one equality constraint. The constraint is that the expander efficiency must follow the data trend of the chosen expander. The expander efficiency can be approximated as a function of V_{ratio} alone as follows:

$$\eta_{exp} = \psi(V_{ratio}, \phi_{ff}) \tag{11}$$

but ϕ_{ff} is mainly a function of the expander shaft speed, which only affects capacity. Therefore, for a fixed capacity,

$$\eta_{exp} \approx \psi(V_{ratio}) \tag{12}$$

Then the constrained optimization problem is posed as

$$\begin{aligned} &\text{Maximize } f(V_{ratio}, \eta_{exp}) = \eta_{cycle,II} \\ &\text{such that } g(V_{ratio}, \eta_{exp}) = \eta_{exp} - \psi(V_{ratio}) = 0 \end{aligned} \tag{13}$$

In general, a necessary condition for the optimum $(V^*_{ratio}, \eta^*_{exp})$ is

$$\nabla f(V^*_{ratio}, \eta^*_{exp}) = \lambda \nabla g(V^*_{ratio}, \eta^*_{exp}), \text{ where } \lambda \in (-\infty, \infty) \tag{14}$$

Feasible directions (which lie on the curve of expander efficiency) are always perpendicular to ∇g, and Equation (14) states that they are also perpendicular to ∇f when cycle efficiency is maximized. This means there is no feasible direction that improves the objective f. However, as in the case of Figure 7, if

$$\left.\frac{\partial g}{\partial V_{ratio}}\right|_{(V^*_{ratio}, \eta^*_{exp})} \neq 0 \Rightarrow \left.\frac{d\eta_{exp}}{dV_{ratio}}\right|_{(V^*_{ratio}, \eta^*_{exp})} \neq 0 \tag{15}$$

then there is a direction which improves η_{exp}. This implies that the expander is underused because the cycle efficiency is not maximized at the maximum expander efficiency. In other words, the expander is poorly matched with the cycle working fluid and operating conditions. The necessary conditions for a matched expander and cycle are: Equation (14) is satisfied and

$$\left.\frac{\partial g}{\partial V_{ratio}}\right|_{(V^*_{ratio}, \eta^*_{exp})} = \left.\frac{\partial f}{\partial V_{ratio}}\right|_{(V^*_{ratio}, \eta^*_{exp})} = 0 \tag{16}$$

This implies that no feasible direction improves $\eta_{cycle,II}$ or η_{exp}, and the peak efficiency of the expander corresponds to the peak efficiency of the cycle using that expander under the given operating conditions.

It would be valuable to know the characteristics of an expander that satisfies Equations (14) and (16). An estimate of the desired expander characteristics can be found by the following procedure: Using a simple thermodynamic model of a Rankine cycle and assumptions about the source and sink temperatures, degrees of subcooling in the condenser, and pump efficiency, generate a set of efficiency curves for the cycle as a function of expansion volume ratio and expander adiabatic efficiency. This is given in Figure 8 where average experimental measurements have been used as inputs to the thermodynamic cycle model.

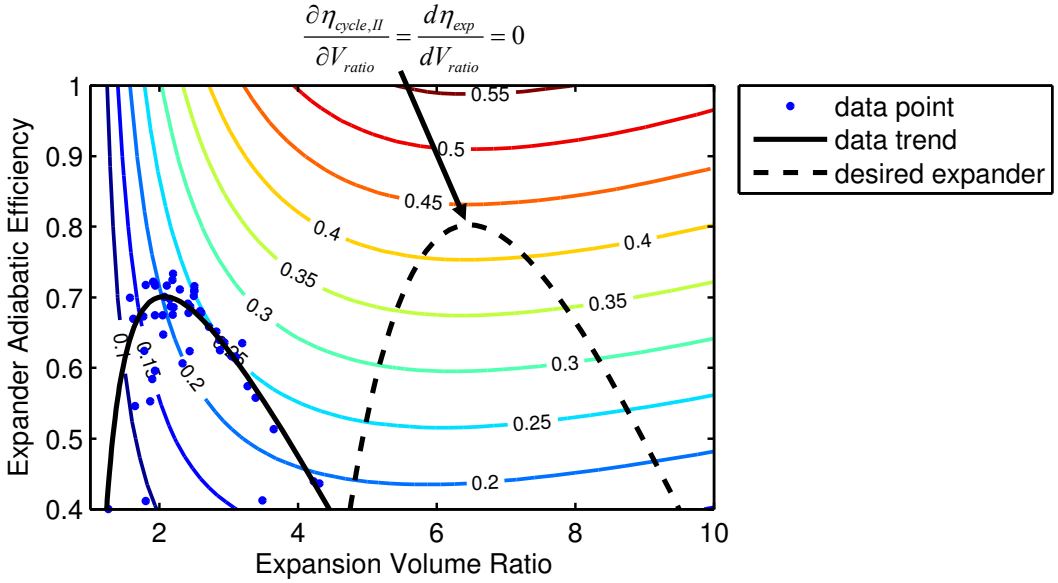

Figure 8: Theoretical ORC cycle efficiency, contours show lines of constant Second Law efficiency as a function of expansion volume ratio and expander adiabatic efficiency, pump adiabatic efficiency of 0.6 is assumed, other cycle inputs are given as the average of measured values, the arrow denotes the point where both cycle and expander efficiency curves have a derivative of zero with respect to volume ratio

The cycle efficiency curves are overlayed with the data for the expander and the performance trend of a desired expander for the operating conditions. For illustrative purposes, the desired expander curve reflects a more optimal design such that the maximum adiabatic efficiency is about 0.80. There is no mismatch between the cycle performance and the expander performance for the hypothetical desired expander – the derivative with respect to expansion volume ratio is zero at the same point for both functions (denoted by the arrow). As a result, an increase in expander efficiency up to its maximum value always results in an increase in cycle efficiency.

According to the results presented in connection with Figure 5b, an expander will perform at peak efficiency when operated at an expansion volume ratio near its built-in volume ratio. Consistent with this observation, the desired expander should have a built-in volume ratio close to 6. The above procedure only aids in the selection of an optimal expander for a single working fluid and set of operating conditions. However, off-design performance can also be predicted by generating a new set of cycle efficiency curves for other operating conditions and superimposing the same expander efficiency curve on the new cycle efficiency curves. If a variable volume ratio expander were used, its volume ratio could be changed to achieve a match between the expander and the cycle over a range of operating conditions.

This result dictates the general suitability of an expander to a given application based on a single characteristic of the expander: its built-in volume ratio. Note that the data shows a relatively flat expander efficiency over a range of volume ratios around the built-in volume ratio (between about 1.5 and 2.5 as seen in Figure 5b for the tested expander). This insensitive region instills confidence that a good match between expander and cycle can be made with knowledge of the expander built-in volume ratio alone.

5. CONCLUSIONS

An ORC with scroll-type expander has been studied experimentally. The data indicates that the adiabatic efficiency of an expander can be characterized by its filling factor and the expansion volume ratio imposed across it. In particular, the data shows that even an off-the-shelf unit, which was not intended for use as an expander, can have promising efficiencies. Peak adiabatic efficiencies occur near a filling factor of unity and an expansion volume ratio near the expander's built-in volume ratio. An expander's suitability in an ORC with a given working fluid and set of operating conditions can be predicted by a straightforward graphical procedure shown in Figure 8. This same technique can be used to aid in the selection of an optimal expander for an ORC with only knowledge of its built-in volume ratio and peak adiabatic efficiency. This approach can be used with a measure of confidence because the expander efficiency is relatively flat with respect to changes in expansion ratio near its built-in volume ratio.

NOMENCLATURE

N	shaft speed	(rev s-1)
P	pressure	(kPa)
$\dot{Q}$	heat transfer rate	(W)
T	temperature	(°C)
V_D	expander displacement	(m3 rev-1)
V_{ratio}	expansion volume ratio	(–)
$\dot{W}$	work rate	(W)
h	specific enthalpy	(J kg-1)
$\dot{m}$	mass flow rate	(kg s-1)
r_v	built-in volume ratio	(–)
s	entropy	(J kg-1 °C-1)
u	uncertainty	
v	specific volume	(m3 kg-1)
η	efficiency	(–)
ϕ_{ff}	expander filling factor	(–)
τ	torque	(N m)

Subscripts

Carnot	Carnot
II	Second Law
R	functional result
comp	compressor
cw	cold water
cycle	for the ORC
dis	expander discharge
exp	expander
evap	evaporator
in	input, inlet
net	net output
pump	pump
s	constant entropy
steam	steam
suc	expander suction
shaft	at the shaft
out	output, outlet
wf	working fluid

REFERENCES

Bell, I., 2011, Theoretical and Experimental Analysis of Liquid Flooded Compression in Scroll Compressors. (Doctoral thesis, Purdue University, 2011).

Figliola, R., Beasley, D., 2006, *Theory and Design for Mechanical Measurements*, John Wiley and Sons, New Jersey, 542 p.

Hugenroth, J., 2006 Liquid Flooded Ericsson Cycle. (Doctoral thesis, Purdue University, 2006).

Lemmon, E., Huber, M., McLinden, M., 2012. NIST Standard Reference Database 23: Reference Fluid Thermodynamic and Transport Properties-REFPROP, Version 9.0, National Institute of Standards and Technology, Standard Reference Data Program, Gaithersburg, 2012.

Lemort, V., Quoilin, S., Cuevas, C., Lebrun, J., 2009, Testing and Modeling a Scroll Expander Integrated into an Organic Rankine Cycle. *Applied Thermal Engineering*. 29. 3094-3102.

ACKNOWLEDGEMENT

The authors would like to thank the Herrick Foundation for sponsorship of this project.

The authors would like to acknowledge the contribution of Wyatt Hodges, who operated the ORC system from May through July 2011 to produce the steady state data points shown in this work.